

Magmatic processes at slow spreading ridges: implications of the RAMESSES experiment at 57° 45' N on the Mid-Atlantic Ridge

M. C. Sinha,¹ S. C. Constable,² C. Peirce,³
A. White,⁴ G. Heinson,⁴ L. M. MacGregor¹ and D. A. Navin³

¹Department of Earth Sciences, University of Cambridge, Bullard Laboratories, Madingley Road, Cambridge, CB3 0EZ, UK. E-mail: sinha@esc.cam.ac.uk

²Institute of Geophysics and Planetary Physics, Scripps Institution of Oceanography, La Jolla, CA 92093-0225, USA

³Department of Geological Sciences, University of Durham, Durham, DH1 3LE, UK

⁴School of Earth Sciences, Flinders University of South Australia, Adelaide 5001, Australia

Accepted 1998 June 23. Received 1998 June 23; in original form 1997 June 26

SUMMARY

This paper is the first in a series of three (this issue) which present the results of the RAMESSES study (Reykjanes Axial Melt Experiment: Structural Synthesis from Electromagnetics and Seismics). RAMESSES was an integrated geophysical study which was carefully targeted on a magmatically active, axial volcanic ridge (AVR) segment of the Reykjanes Ridge, centred on 57°45'N. It consisted of three major components: wide-angle seismic profiles along and across the AVR, using ocean-bottom seismometers, together with coincident seismic reflection profiles; controlled-source electromagnetic sounding (CSEM); and magnetotelluric sounding (MT). Supplementary data sets included swath bathymetry, gravity and magnetics.

Analyses of the major components of the experiment show clearly that the sub-axial geophysical structure is dominated by the presence and distribution of aqueous and magmatic fluids. The AVR is underlain by a significant crustal magma body, at a depth of 2.5 km below the sea surface. The magma body is characterized by low seismic velocities constrained by the wide-angle seismic data; a seismic reflection from its upper surface; and a region of anomalously low electrical resistivity constrained by the CSEM data. It includes a thin, ribbon-like melt lens at the top of the body and a much larger region containing at least 20 per cent melt in a largely crystalline mush zone, which flanks and underlies the melt lens. RAMESSES is the first experiment to provide convincing evidence of a significant magma body beneath a slow spreading ridge. The result provides strong support for a model of crustal accretion at slow spreading rates in which magma chambers similar to those at intermediate and fast spreading ridges play a key role in crustal accretion, but are short-lived rather than steady-state features. The magma body can exist for only a small proportion of a tectono-magmatic cycle, which controls crustal accretion, and has a period of at least 20 000 years. These findings have major implications for the temporal patterns of generation and migration of basaltic melt in the mantle, and of its delivery into the crust, beneath slow-spreading mid-ocean ridges.

Key words: electromagnetic surveys, magma chamber, magnetotellurics, mid-ocean ridge, seismic structure.

1 INTRODUCTION AND RATIONALE

It has been known for at least two decades that oceanic lithosphere, and in particular oceanic crust, displays a considerable degree of uniformity irrespective of the detailed properties of the spreading ridge at which it formed. For example, neither the seismically determined structure and thickness (reviewed

by White, McKenzie & O'Nions 1992) nor the major element composition determined from basaltic lavas (reviewed by Sinton & Detrick 1992) of oceanic crust shows strong trends between different ocean basins (e.g. Atlantic and Pacific), even if the basins were formed by different ridge systems and at different spreading rates. This broad similarity contrasts with the obvious and systematic structural differences between the

spreading centres themselves; for example, whether the axes are marked by topographic highs or by median valleys. Early explanations (e.g. Cann 1974) for the composition and layering of oceanic crust drew heavily on observations of ophiolites, and postulated the existence of large crustal magma chambers beneath ridge axes. The importance of this concept is that a magma chamber provides a setting in which the gradual crystallization of an initially primitive melt can lead to the range of observed petrologies (e.g. Sinton & Detrick 1992); it provides a reservoir from which melt can be injected into the newly forming crust as dykes or erupted onto the seafloor as lavas; and it provides a location from which deeper crustal rocks can form by a process of slow crystallization. It thus provides plausible explanations for many of the lithological and structural features observed both in young oceanic crust and in ophiolites. Consequently, the absence of any direct geophysical evidence for crustal magma bodies beneath slow-spreading ridges—especially when it is combined with evidence (e.g. Smith & Cann 1992) that volcanic construction involves, at least in some places, not a single large magma body but many very small, isolated melt bodies—poses some difficult questions about the formation of oceanic crust and the broad uniformity of its composition and layering. Do we observe the latter because, despite variations, all ridges generate crust by processes that have in common the role played by a significant crustal melt body? Or does the broad similarity tell us nothing about the construction of the crust, since neither compositional nor structural (seismic layering) properties result from a shared mode of construction at the ridge axis?

Many previous geophysical studies have provided seismic constraints on the geometry and properties of crustal magma chambers beneath the faster spreading ridges in the Pacific (e.g. Detrick et al. 1987, 1993; Harding et al. 1989; Vera et al. 1990; Collier & Sinha 1992a,b), and have been influential in the development of models for the magmatic accretion of crystalline oceanic crust at spreading rates of greater than about 60 mm a^{-1} (e.g. Henstock, Woods & White 1993). However, there has been only one report of direct geophysical evidence for a crustal melt body beneath a slow spreading ridge (Calvert 1995, 1997). This observation relies on faint reflections seen on a carefully processed, multi-channel seismic reflection profile. The apparent reflector is only present over a limited area, and the interpretation suffers from the fact that the same data had been previously reported as indicating that there was no melt body at that location (Detrick et al. 1990). Other geophysical experiments at many locations on slow spreading ridges (e.g. Fowler 1976; Fowler & Keen 1979; Purdy & Detrick 1986; Bunch & Kennett, 1980; Smallwood, White & Minshull 1995; Wolfe et al. 1995) have found no evidence for a significant crustal melt body. Arguments based on thermal modelling have long shown that the heat flux into the crust associated with magma delivery from the mantle is insufficient to maintain a steady-state crustal melt body, even of small dimensions, at slow spreading rates (e.g. Sleep 1975; Kuszniir & Bott 1976). Current understanding of the importance and efficiency of hydrothermal circulation systems in removing heat from the axial crust serve only to make these thermal arguments more compelling.

One way of resolving the apparent contradiction between the need for crustal melt bodies to explain structural and petrological observations and the geophysical evidence that in most places they are not present is the proposition that,

beneath slow spreading ridges, crustal magma chambers are transient or ephemeral features. If this were the case, then the process of magmatic accretion at slower spreading rates would have to be episodic or cyclic, and observations of crustal melt bodies would rely on identifying a spreading segment that was at the appropriate stage of its life cycle. Questions of how the processes of crustal growth depend on spreading rate could then be posed in terms of whether accretion involves a melt body of broadly similar geometry at all spreading rates, with the major differences being confined to the temporal variability of the process (short-lived, transient melt bodies at slow rates, compared with long-lived or steady-state bodies at faster rates), or whether the geometry and, indeed, the existence of the melt body, and hence the whole mechanism of crustal accretion and the architecture at all scales of the crystalline crust, differ for fast and slow spreading ridges.

This and the two following papers detail the results of a carefully targeted, multi-component, geophysical experiment carried out near the southern end of the slow spreading Reykjanes Ridge in the northern North Atlantic ocean. RAMESSES (Reykjanes Axial Melt Experiment: Structural Synthesis from Electromagnetics and Seismics) is the first major study of an active spreading centre to have been designed from the outset as a multi-component project, combining electromagnetic and seismic techniques in a single, integrated investigation. The experiment consisted of three major components: seismic wide-angle and normal-incidence profiles along and across the ridge axis, to determine crustal thickness and seismic structure; controlled-source electromagnetic sounding along and across the axis, to constrain the electrical resistivity structure of the crust; and magnetotelluric sounding, to constrain the deeper electrical resistivity structure of the upper mantle.

Seismic and electromagnetic studies were selected as complementary techniques because of the different strengths that each brings to the experiment as a whole. Seismic methods provide unrivalled structural resolution of crustal features and of the crust–mantle boundary. In contrast, electromagnetic methods are relatively insensitive to sharp structural boundaries, but are sensitive to the large-scale distribution of crustal temperature and to the presence, amount and interconnectivity of conductive crustal fluids. In combination, the two techniques provide the most powerful geophysical means available for constraining and characterizing structures within the lithosphere that relate to magma generation, migration and emplacement, and to crustal growth and evolution.

The site of the RAMESSES experiment was carefully chosen in order to locate it over a spreading segment that is currently at an unusually magmatically vigorous stage in its development. RAMESSES provides the first reliable evidence for the presence of a substantial crustal melt accumulation beneath a slow spreading ridge, and preliminary results from the study were presented by Sinha et al. (1997). In this paper, we describe how the components of the experiment relate to each other, and present conclusions from our attempt to synthesize the results of the experiment as a whole. Detailed accounts of two of the three data sets (seismic and CSEM) that constitute the major components of RAMESSES, and of their individual analyses and interpretations, are given in the accompanying papers: Navin et al. 1998 (RAMESSES II) and MacGregor, Constable & Sinha 1998 (RAMESSES III), this issue. The results allow us to make significant progress towards

understanding melt generation, delivery and emplacement processes at slow spreading mid-ocean ridges, and the similarities and differences when compared with those at faster spreading ridges.

2 EXPERIMENT LOCATION AND GEOLOGICAL SETTING

The Reykjanes Ridge (Fig. 1) provided a suitable location for this study for two reasons. First, the pattern of along-axis segmentation had already been clearly documented by a number of previous studies. Second, in contrast to most slow spreading parts of the ridge system, the Reykjanes Ridge has relatively subdued topography for its spreading rate (20 mm a⁻¹ full rate). Since the techniques used in this study are susceptible to degradation of their resolving power in the presence of severe topography at the seafloor (e.g. Detrick et al. 1990; Unsworth 1994), the Reykjanes Ridge makes an attractive target for high-resolution seismic and electromagnetic investigations.

At its northern end, the Reykjanes Ridge is profoundly affected by the proximity of the Iceland hot spot: this results

in anomalously shallow water depths, the absence of a median valley, and a crustal geochemistry that shows a strong plume signature. The hot-spot influence decreases with increasing distance from Iceland, with both the geochemical and bathymetric anomalies declining steadily (Schilling et al. 1983; Keeton et al. 1996), although different geochemical tracers exhibit somewhat variable behaviour with increasing distances from the hot-spot centre (Taylor et al. 1995). A discernible rift valley appears south of about 58°40'N. For the whole length of the Reykjanes Ridge, along-axis segmentation takes the form of a series of en echelon, overlapping, axial volcanic ridges (AVRs). The elongated AVRs have typical dimensions of up to a few tens of kilometres in length, and are arranged so that the offsets between them are all right-lateral (Searle & Laughton 1981; Searle, Field & Owens 1994; Keeton et al. 1996). Individual AVRs are aligned approximately orthogonal to the spreading direction of 096° (DeMets et al. 1990), but the overall trend of the ridge (approximately 035°) is oblique to the spreading direction. There are no transform offsets of the axis between 57°N (the Bight fracture zone) and the Reykjanes Peninsula—a distance of almost 950 km. Side-scan sonar imagery of the seafloor at the axis of the Reykjanes

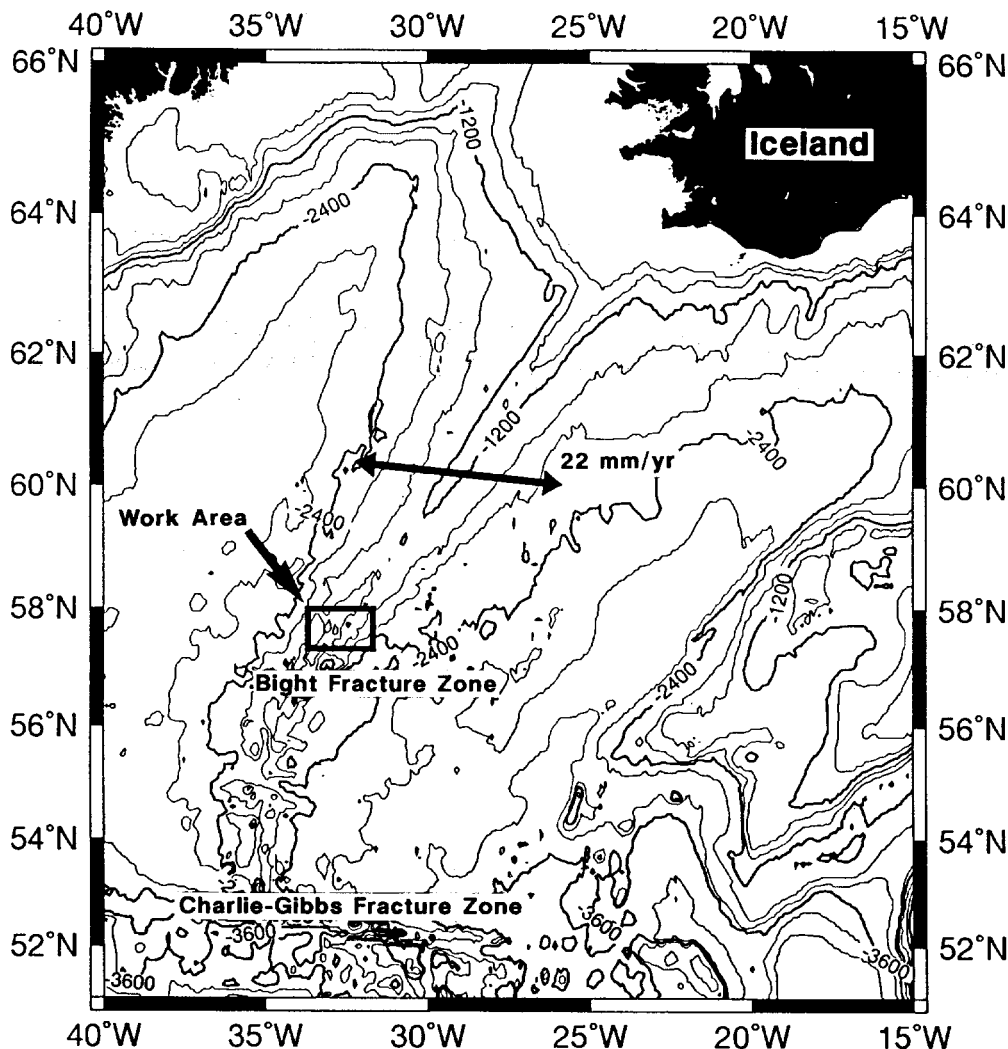


Figure 1. Bathymetry of the North Atlantic region, and the location of the RAMESSES study area (solid box) on the axis of the Reykjanes Ridge. Arrows show the direction of seafloor spreading at the ridge. Bathymetric contours from the ETOPO-5 data set are shown at 400 m intervals.

Ridge (Murton & Parson 1993) reveals a complex interplay between constructive volcanism (leading to the construction of AVRs), tectonic extension (leading to the break-up of AVRs by normal faults aligned orthogonally to the spreading direction), and, at distances of more than about 700 km from Iceland, the development of major inward-facing normal faults that run sub-parallel to the overall trend of the ridge and form the bounding walls of the developing median valley. Comparisons among AVRs reveal that constructive volcanism dominates at some, while at others there is little evidence of recent magmatism, and tectonic features dominate. This observation has led to the inference that AVRs follow a life cycle in which occasional influxes of magma from the mantle are separated by long periods of magmatic dormancy (Parson et al. 1993).

Within the Reykjanes Ridge, we selected a particular AVR segment at $57^{\circ}45'N$, based on comparisons of high-resolution, deep-towed side-scan sonar imagery of volcanic and tectonic features at the seafloor (Fig. 2). The AVR chosen for the RAMESSES study extends along an approximately N–S trend for some 35 km, between $57^{\circ}33'N$ and $57^{\circ}53'N$. It is located approximately 120 km south of the first appearance, heading away from Iceland, of a discernible median valley, and approximately 1100 km from the centre of the Iceland plume. It lies immediately south of an unusually large offset between adjacent AVRs (Searle et al. 1994). Our selection was based on an assumption that the AVR will be undergoing vigorous volcanic construction at the point in time when the rate of melt injection into the crust (and hence the likelihood of finding a crustal melt reservoir) reaches its maximum. In contrast, a more mature AVR that has reached its full topographic development is probably already at the end of the magmatically robust phase of its life cycle. This model was based on analogies with the pattern of tectono-magmatic cycles, and their effects on seafloor volcanic construction and the width and brightness of the crustal magma chamber reflector, previously inferred at the intermediate spreading rate Valu Fa Ridge in the southern Lau Basin (Collier & Sinha 1992a,b). We therefore selected the AVR which showed the greatest evidence of fresh volcanic construction (hummocky topography, bright back-scattering and fresh-looking lava flows extending for distances of several kilometres), and the least evidence of the recent normal faulting and fissuring that characterizes most AVRs, and that appears to indicate post-magmatic, tectonic extension. By comparison with a number of other larger AVRs, which we interpret as being at or close to the end of the magmatically robust stage of their lives, our selected AVR is a relatively unimpressive feature topographically, although we believe it to have recently started a phase of rapid growth by volcanic construction.

The shape of the RAMESSES AVR and its relation to the median valley and the larger-scale structure of the ridge can be seen clearly in Fig. 3. The AVR is outlined by the 1800 m bathymetric contour. It sits in the bottom of the median valley, is 4 to 5 km wide at its base, and is over 30 km long. Its summit lies at a depth of less than 1600 m, while the median valley adjacent to it mostly lies at a maximum depth of 2000 to 2100 m. The shallowest point on the AVR is close to $57^{\circ}45'N$. North of this, the AVR gradually becomes both narrower and deeper until near $57^{\circ}50'N$, where a sub-circular volcanic high marks its northern limit. To the south, the AVR becomes bifurcated south of $57^{\circ}42'N$, but can still be identified as a bathymetric feature as far south as $57^{\circ}36'N$. The median

valley, as outlined by the 1800 m contour, reaches its narrowest point close to the centre of the AVR, and widens considerably to the north and south, beyond the ends of the AVR. The offsets between the AVR and adjacent spreading segments to the NNE and SSW are both marked by deep basins reaching water depths of more than 2300 m. The southern end of the AVR lies very close to the eastern edge of the median valley, which is marked here by a major fault scarp running approximately orthogonal to the spreading direction, and parallel to the AVR. At its northern end, the AVR is located close to the centre of the median valley, and here the western edge of the valley is also marked by a major, spreading-orthogonal fault scarp. South of $57^{\circ}40'N$, north of $57^{\circ}49'N$, and further than about 15 km from the axis, the trend of the major bathymetric features is close to the overall trend of the Reykjanes Ridge (035°). Minimum depths on the flanks of the ridge are reached at about 15 km off-axis; on the eastern flank they are less than 1000 m, although 1200 m is more common. Thus the median valley at this point on the ridge is typically about 30 km wide between the highest points, and typically 800 to 1000 m deep, with the AVR centred in its narrowest point and rising to up to 500 m above the valley floor.

3 EXPERIMENTAL DESIGN

The study was designed to provide coincident determinations of electrical resistivity and P- and S-wave velocities in the crust beneath the AVR, and of deeper resistivity in the upper mantle. Experimental work was carried out in 1993 October–November, during cruise CD 81/93 of RRS Charles Darwin (Sinha et al. 1994). The seismic component (RAMESSES II) consisted primarily of two wide-angle seismic profiles along and across the axis of the AVR (Fig. 3). Each profile was shot twice, first with chemical explosives at 1 or 2 km shot spacings and second with a large-volume airgun array at approximately 100 m shot spacings. The receivers were an array of 10 digital ocean-bottom seismographs (OBSs) from the universities of Durham and Cambridge. Seismic reflection data were also collected along both of these profiles and along two further across-axis profiles, using a short (800 m), multi-channel hydrophone streamer. The seismic profiles extended to distances of 32 km WNW and 67 km ESE of the axis—corresponding to crustal ages of 2.6 and 5.5 Ma, respectively. Wide-angle arrivals are observed in the resulting data at all ranges up to 90 km on the across-axis profile, and 35 km on the along-axis profile. They provide dense coverage of crossing ray paths at all crustal depths, as well as reflected and refracted arrivals from the uppermost mantle.

The controlled-source electromagnetic (CSEM) component (RAMESSES III) was essentially coincident with the central part of the seismic experiment, so far as the differing source–receiver geometries required for the two techniques allows. CSEM signals were transmitted along two source tows, both parallel to the AVR axis, using the University of Cambridge DASI deep-towed transmitter system (Sinha et al. 1990). Useful data were recorded by three Scripps ELF instruments (Constable & Cox 1996), which each recorded two orthogonal components of horizontal electric field. In young oceanic lithosphere where crustal resistivities are low, CSEM signals cannot be transmitted to such great ranges as seismic signals from explosive shots or airgun arrays, so the CSEM component investigated only the structure close to the axis. The CSEM

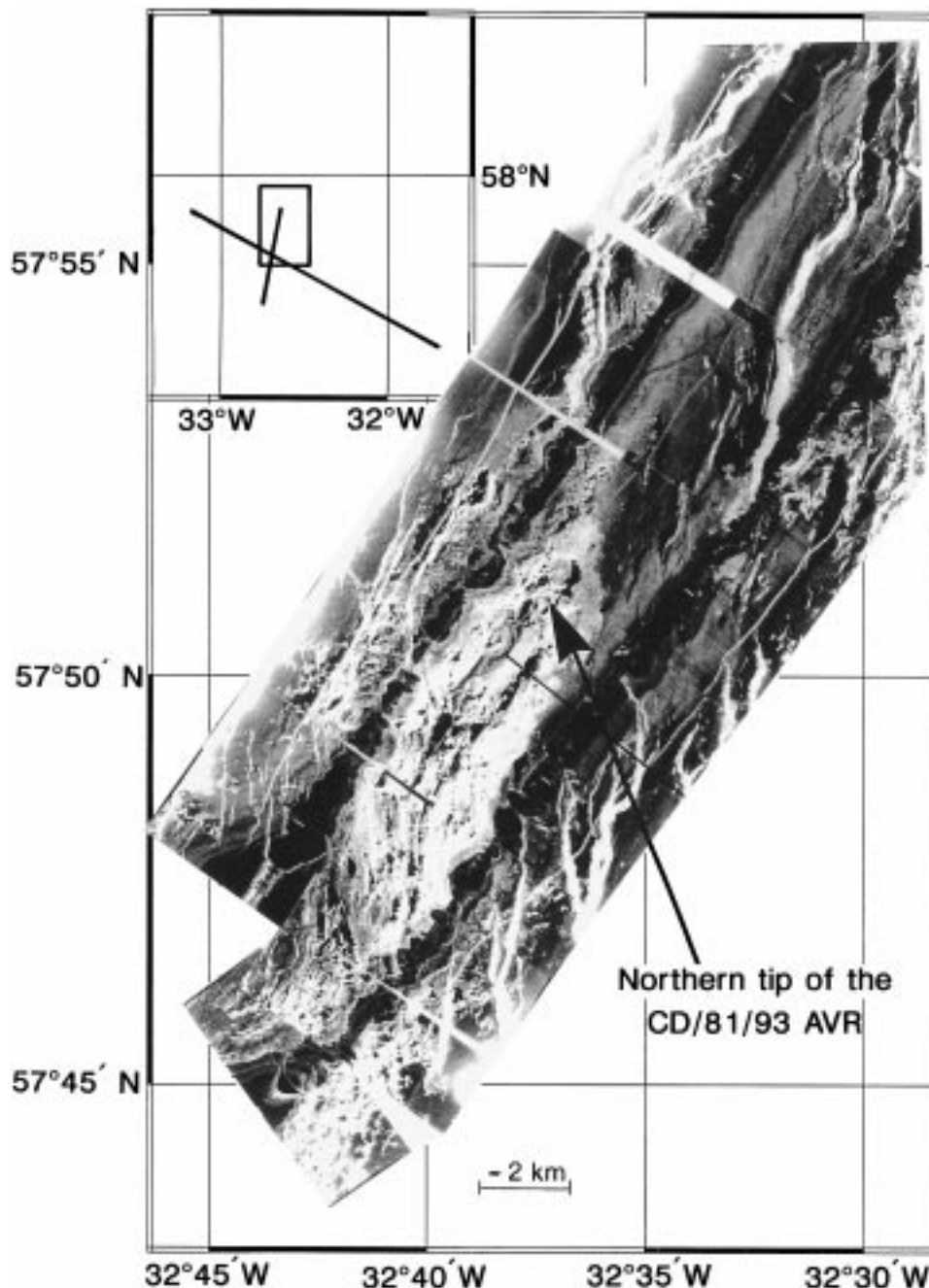


Figure 2. TOBI high-resolution, deep-towed side-scan sonar mosaic of the seafloor along the northern part of the RAMESSES AVR, after Parson et al. (1993). Light shades indicate strong back-scattering from rough seafloor, while darker shades indicate weak back-scattering from smooth (typically sediment-covered) seafloor. The bright back-scattering and constructional volcanic features of the AVR itself can be seen to truncate (and so can be inferred to overlie and post-date) the many sinuous reflectors that correspond to surface traces of faults. The inset shows the position of the main panel with respect to the two (along- and across-axis) wide-angle seismic profiles of the RAMESSES experiment.

data provide constraints on crustal resistivity over a zone extending for approximately 5 km to either side of the AVR axis (corresponding to a crustal age of 0.5 Ma), and to a depth of between 4 and 6 km below the seafloor.

For the magnetotelluric (MT) experiment, low-frequency, horizontal electric field data were collected at six sites at distances of up to 30 km from the AVR axis, and three-component magnetic field data were recorded at three sites at up to 15 km from the axis (Heinson et al., in preparation; Sinha et al. 1997). A combined magnetic and electric field

instrument was used at one of the sites, located on the centre of the AVR, at the intersection of the two wide-angle seismic profiles. Although the MT component has the lowest spatial resolution of any part of the overall experiment, it also has the deepest penetration. By deploying the MT instruments immediately on arrival at the work area, and recovering them last before leaving, it proved possible to obtain MT estimates for the period range 100 to 10 000 s, resulting in a data set that provides constraints on resistivity to a depth of at least 150 km beneath the seafloor.

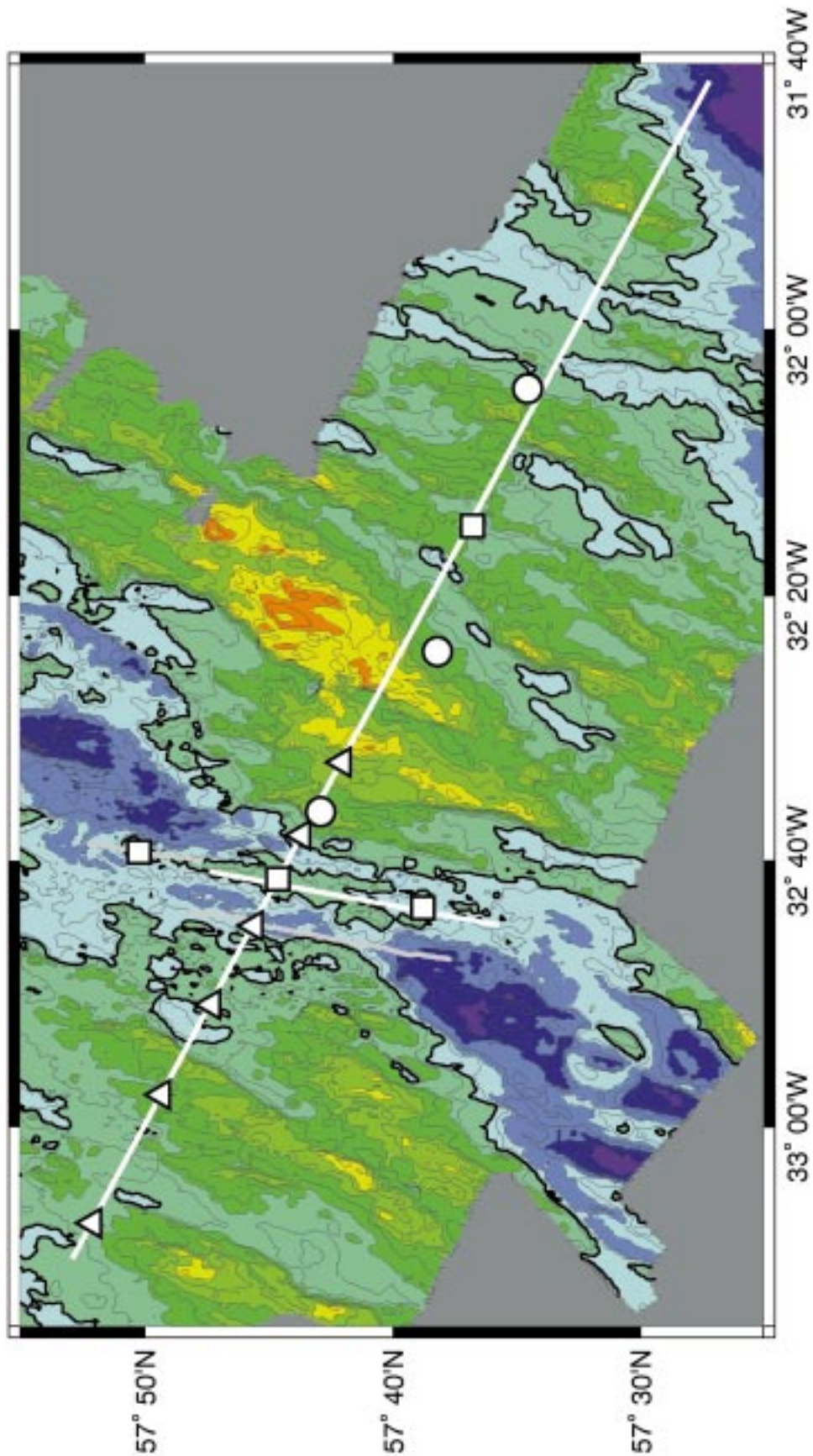


Figure 3. Swath bathymetry of the study area, and locations of major components of the RAMESES experiment. Bathymetric contour interval is 100 m. The 1800 m contour is shown in bold, and outlines the inner walls of the median valley and the AVR. Solid white lines mark the locations of the two wide-angle seismic profiles. Grey lines mark the two transmitter tows of the CSEM component. Triangles: positions of ocean-bottom seismic recorders; circles: positions of ocean-bottom electromagnetic instruments; squares: locations that were occupied by both a seismic and an electromagnetic instrument. Only instruments that provided useful data are shown.

Supplementary data collected as part of RAMESSES include 100 per cent swath bathymetric coverage over an area of the order of 12 000 km², and allow the three primary data sets to be interpreted within a detailed contextual understanding of the larger-scale structure of this part of the Reykjanes Ridge. The swath bathymetry data have contributed to a larger compilation, covering virtually the entire Reykjanes Ridge (Keeton et al. 1997).

4 A STRUCTURAL MODEL OF THE 57°45'N AVR

In this section, we summarize the main structural features of the 57°45'N segment of the Reykjanes Ridge in terms of the geophysical parameters (seismic velocities and boundaries, and electrical resistivities) determined by the experiment and detailed in the accompanying papers. In Section 5, we shall discuss the observed structures in terms of their implications for the presence of magmatic and other fluids, and the possible processes involved in lithospheric accretion.

4.1 Off-axis crustal structure

Fig. 4(a) shows a set of seismic P-wave velocity versus depth curves derived from analysis of the OBS data recorded on the across-axis wide-angle profile. At distances greater than about 15 km from the axis, the crust exhibits a typical oceanic structure, constrained in the seismic data by crustal and upper-mantle diving rays (P_{c}^{u} and P_{c}^{m}) and by wide-angle reflections from the Moho (P_{c}^{m}). Velocities are low in the uppermost crust, but increase rapidly with depth—from about 2.5 km s⁻¹ at the seafloor to around 4.5 km s⁻¹ at depths of less than 1 km, and to well over 6 km s⁻¹ by the base of seismic layer 2, which occurs at 2 to 2.5 km depth below the seafloor. In seismic layer 3, velocity continues to increase with depth, but the gradient is much lower so that the P-wave velocity reaches approximately 7 km s⁻¹ just above the Moho. The Moho transition occurs at between 7 and 7.5 km depth. The seismic data are consistent with a sharp transition from crust to uppermost mantle, and with an upper-mantle velocity of between 7.9 and 8.2 km s⁻¹. The crustal thickness, crustal velocities and crustal velocity gradients are entirely consistent with the range of 'normal' oceanic crust in either the Atlantic or Pacific oceans as compiled by White et al. (1992).

Away from the AVR axis, the electromagnetic data do not provide strong constraints on the electrical resistivity structure. The CSEM results are, however, consistent with shallow crustal resistivities of between 10 and 100 V m, increasing to at least 200 V m in the lower crust.

4.2 The upper crust beneath the AVR

The seismic velocity structures derived from both the along-axis and across-axis wide-angle profiles show a marked decrease in P-wave velocity in the upper-crustal layer (layer 2) within 10 km of the axis, compared with velocities at similar depths at greater distances from the axis (Fig. 4b). Although velocities directly below the seafloor do not differ markedly from those off-axis, the velocity gradient in layer 2 is significantly lower close to the axis, so that, by the base of layer 2, velocities are typically 0.8 km s⁻¹ slower than at the same depth off-axis. This structure is consistent with the CSEM results, which

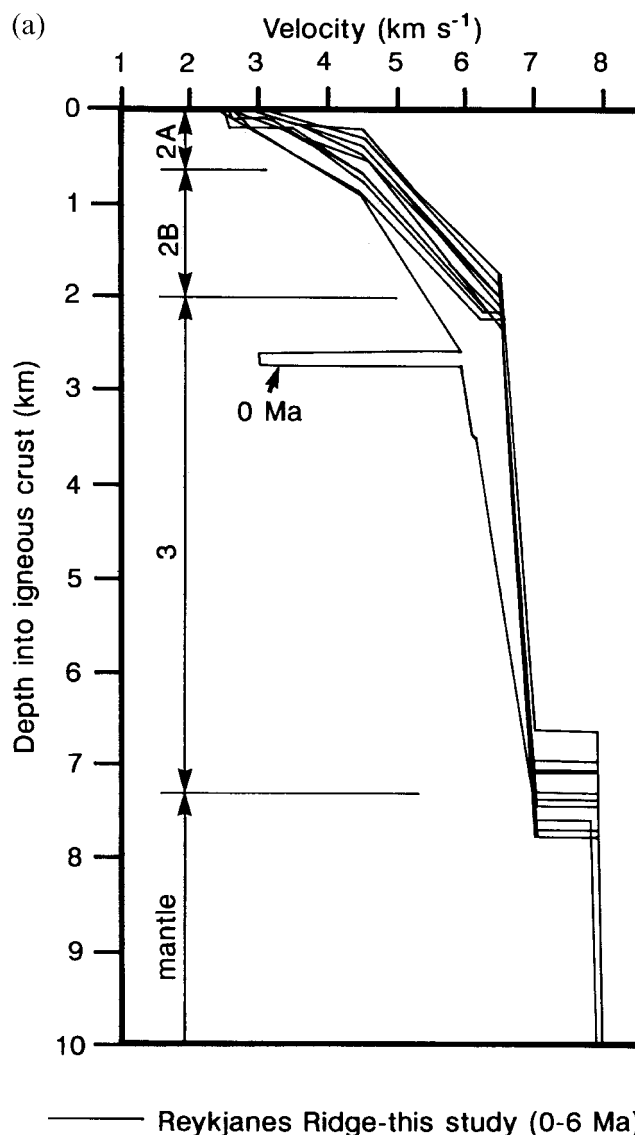


Figure 4. (a) P-wave velocity versus depth curves from the final across-axis wide-angle seismic model. Curves are shown at 10 km increments along the profile. The structure beneath the AVR axis is labelled '0 Ma'. (b) Across-axis variation in seismic P-wave velocity beneath the AVR, from the final seismic model. Contours indicate the reduction in P-wave velocity relative to the mean velocity at the same depth into the crust for the off-axis structure. Contour interval 0.1 km s⁻¹. (c) Across-axis resistivity structure, showing the same region as (b), based on the final CSEM model. Resistivities in V m. S1 and S2 are the locations of the source tows.

provide good constraints on upper-crustal resistivity beneath the AVR itself (Fig. 4c). At the axis, the resistivity of the uppermost crust is very low—only about 1 V m—indicative of very high, interconnected porosity saturated with conductive sea water. Resistivity increases with depth beneath the AVR, reaching around 10 V m in the top 500 m of the crust, and around 40 V m at depths of 1 to 2 km.

4.3 Axial melt lens

One of the most striking features of the seismic interpretation is the inferred presence of a thin lens of material with extremely

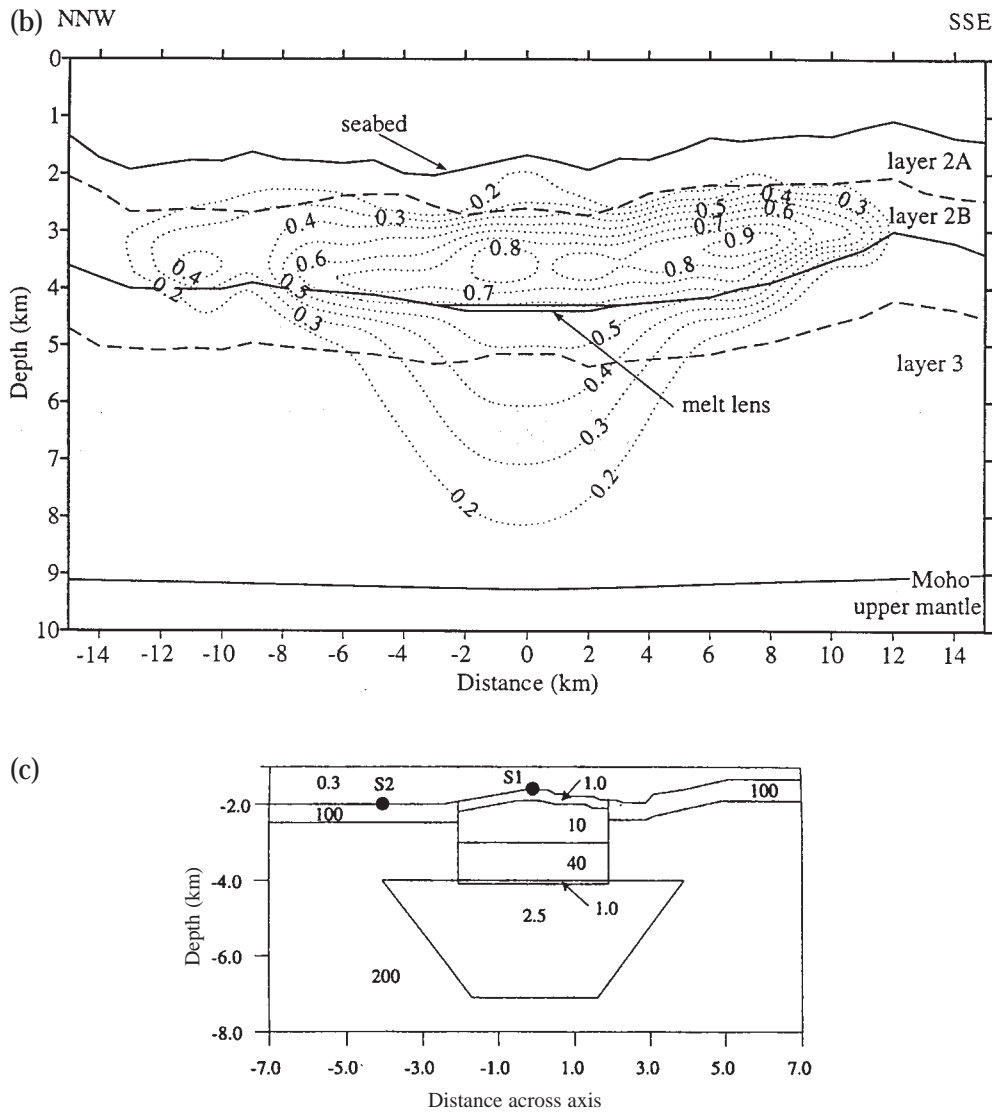


Figure 4. (Continued.)

low P-wave velocity (3 km s^{-1}), interpreted as a zone of pure basaltic melt, at a depth of just over 2 km beneath the AVR axis. This feature is required by the seismic data, in order to fit the amplitude behaviour of crustal diving rays which intersect it on both the along- and across-axis seismic profiles. Specifically, in the along-axis seismic data, there is a sharp reduction in the amplitudes of crustal diving-ray arrivals at an offset of approximately 12 km, indicative of a shadow zone caused by a low-seismic-velocity layer. Low-amplitude arrivals at longer ranges in the same data indicate that the low-velocity layer can have only a limited depth extent. Similarly, on the across-axis wide-angle seismic record sections, low amplitudes are observed in a shadow zone close to the axis for rays passing through the crust at the depth of the implied low-velocity layer. In the preferred, final, seismic model, which fits both the along-axis and across-axis wide-angle data, this feature is 100 m thick, 4 km wide, and extends for virtually the entire along-axis length of the AVR. We interpret this feature as a thin, ribbon-like lens of basaltic melt. It is strikingly similar to the melt lens imaged beneath parts of the East Pacific Rise and Valu Fa Ridge, although at 4 km wide it is at

the upper end of the range of widths observed at higher spreading rates.

4.4 Underlying low-velocity and low-resistivity zone

Occupying a much larger volume than the melt lens, and flanking and underlying it, is a region with more moderately but nonetheless substantially reduced seismic velocities. This region, which extends from the base of the melt lens to within 1 km of the Moho—6 km below the sea surface—and over a width across-axis of at least 10 km, is well constrained by the traveltimes of many crossing ray paths of lower-crustal diving waves in the across-axis seismic profile, and by the traveltimes of low-amplitude (but clear) first arrivals in the along-axis seismic data, recorded at ranges greater than the sharp drop in amplitudes caused by the velocity inversion. Within this region, P-wave velocities are reduced by at least 0.2 km s^{-1} , and by up to 0.5 km s^{-1} .

The presence of an extensive body with anomalous physical properties at this depth beneath the AVR is confirmed by the CSEM data. These data show significant 'splitting' of the

observed amplitudes of CSEM signals at source–receiver ranges of 5 to 15 km, from along-ridge transmissions as compared with across-ridge transmissions. Such splitting of radial and azimuthal (with respect to the transmitter orientation) field amplitudes is characteristic of the presence of a sharp drop in resistivity with depth beneath the CSEM experiment, and the CSEM data cannot be explained by models that lack a substantial region of very low resistivity in the mid-crust. Given the superior spatial resolution of the seismic method, the final model from the CSEM analysis has been constrained to have the top of the low-resistivity anomaly coincident with the top of the seismic low-velocity zone. Additionally, in the final CSEM model, a lens-shaped feature, consistent with the seismically determined melt lens, has also been included, and has been assigned a resistivity appropriate for pure basaltic melt. While the CSEM data lack the spatial resolution to distinguish the melt lens from the larger low-resistivity anomaly, the inclusion of the lens in the final CSEM model achieves two objectives. First, it makes the two models structurally consistent. Second, its inclusion allows an assessment to be made of the maximum resistivity (i.e. minimum deviation from background resistivity) required in the larger region to satisfy the constraints of the data. In the final CSEM model, a volume corresponding to the -0.3 km s^{-1} or less P-wave velocity anomaly is shown to have a resistivity of no more than about 2.5 V m —dramatically lower than the 200 V m typical of mid to lower crust away from the axis. We interpret this combined seismic and resistivity anomaly as a zone of partially crystallized melt, in the form of a crystal mush zone.

4.5 The Moho and crustal thickness

It is important to note that the seismic data—both P and P_P arrivals—constrain the crustal thickness beneath this part of the North Atlantic to be between 7 and 7.5 km. This is comfortably within the range of normal crustal thickness for both Atlantic and Pacific oceanic crust, away from hot spots and ridge offsets (White et al. 1992). This indicates that, although the Iceland hot spot clearly has an influence on seafloor spreading here, as evidenced by the subdued median valley topography and anomalously shallow water depths, that influence does not result in an increased crustal thickness, and so cannot be related to any increase in the overall melt production rate here compared to ‘normal’ oceanic crust. The data cannot resolve whether there are variations in crustal thickness in the along-axis direction. Across-axis, it is possible that the crust is slightly thicker, by about 500 m, beneath the AVR than at greater ages, but this is at the limit of resolution of the seismic data. The Moho appears to be well developed as a sharp interface, or at least to occur over a vertical distance small compared with a seismic wavelength (which is about 1 km at that depth) at all distances across-axis, including directly beneath the AVR, from where P_P reflections are observed.

4.6 Along-axis variations

Fig. 4 shows only variations in structure that occur vertically and across-axis. The geophysical data provide fewer constraints on along-axis variations in structure. There are, however, some conclusions that can be drawn. First, seismic reflection data

from the along-axis profile show two weak, intra-crustal reflectors that do not appear to be due to out-of-plane reflections from the rough seafloor. These are interpreted as the reflection from the top of the melt lens, and a pegleg multiple of the same event, reflected once at the seafloor. One or the other of these reflections is weakly visible almost continuously along a 20 km length of the profile, suggesting that the crustal melt lens is continuous along-axis beneath much of the AVR. The CSEM data, too, would be sensitive to along-axis breaks in the connected melt phase in the underlying crystal mush zone. CSEM modelling suggests that the mush zone must be continuous at least beneath the northern half of the AVR.

4.7 Upper-mantle structure

The CSEM data are not sensitive to structure below the base of the crystal mush zone. The wide-angle seismic data constrain the P-wave velocity in the uppermost mantle, but none of the observed arrivals has penetrated to more than a few kilometres beneath the Moho. In contrast, the MT data provide constraints on resistivity to a depth of at least 120 km, as reported in Sinha et al. (1997).

An important conclusion from the published MT interpretation is that between about 10 and 50 km below the sea surface—that is, in the top 40 km of the upper mantle—a relatively resistive region is sandwiched between less resistive layers above and below it. The upper low-resistivity layer corresponds to the crust. The deeper low-resistivity layer, at depths of between 50 and 100 km below sea level, is characterized by resistivities of 20 V m or less. We interpret this deep zone as containing a small, but interconnected, partial melt phase resulting from decompression partial melting. The resistive, middle layer of the sandwich extends from less than 20 km depth to at least 40 km depth, and is characterized by resistivities as high as 500 V m (Sinha et al. 1997). This is close to the resistivity that would be expected for dry olivine at a temperature of 1350°C (Constable, Shankland & Duba 1992) and so suggests that the top 40 km of the mantle contains essentially no interconnected melt phase. This observation is entirely compatible with the normal upper-mantle P-wave velocities (7.9 to 8.2 km s^{-1}) and sharp Moho discontinuity, even directly beneath the AVR axis, required by the seismic data.

5 STRUCTURES, FLUIDS AND THEIR IMPLICATIONS FOR CRUSTAL AND LITHOSPHERIC ACCRETION PROCESSES

Taken together, the structural observations outlined in Section 4 and justified in detail in the accompanying papers have important implications for the way in which new oceanic crust is formed by melt generation, migration and emplacement beneath the Reykjanes Ridge at $57^\circ 45' \text{N}$. Fig. 5 presents a self-consistent synthesis of the structural constraints along a profile across the centre of the AVR, based on all the component parts of the geophysical experiment. The inferred structure is drawn along a cross-section coincident with the across-axis wide-angle seismic profile. Note that there is a break in scale on the depth axis, at 10 km below the sea surface.

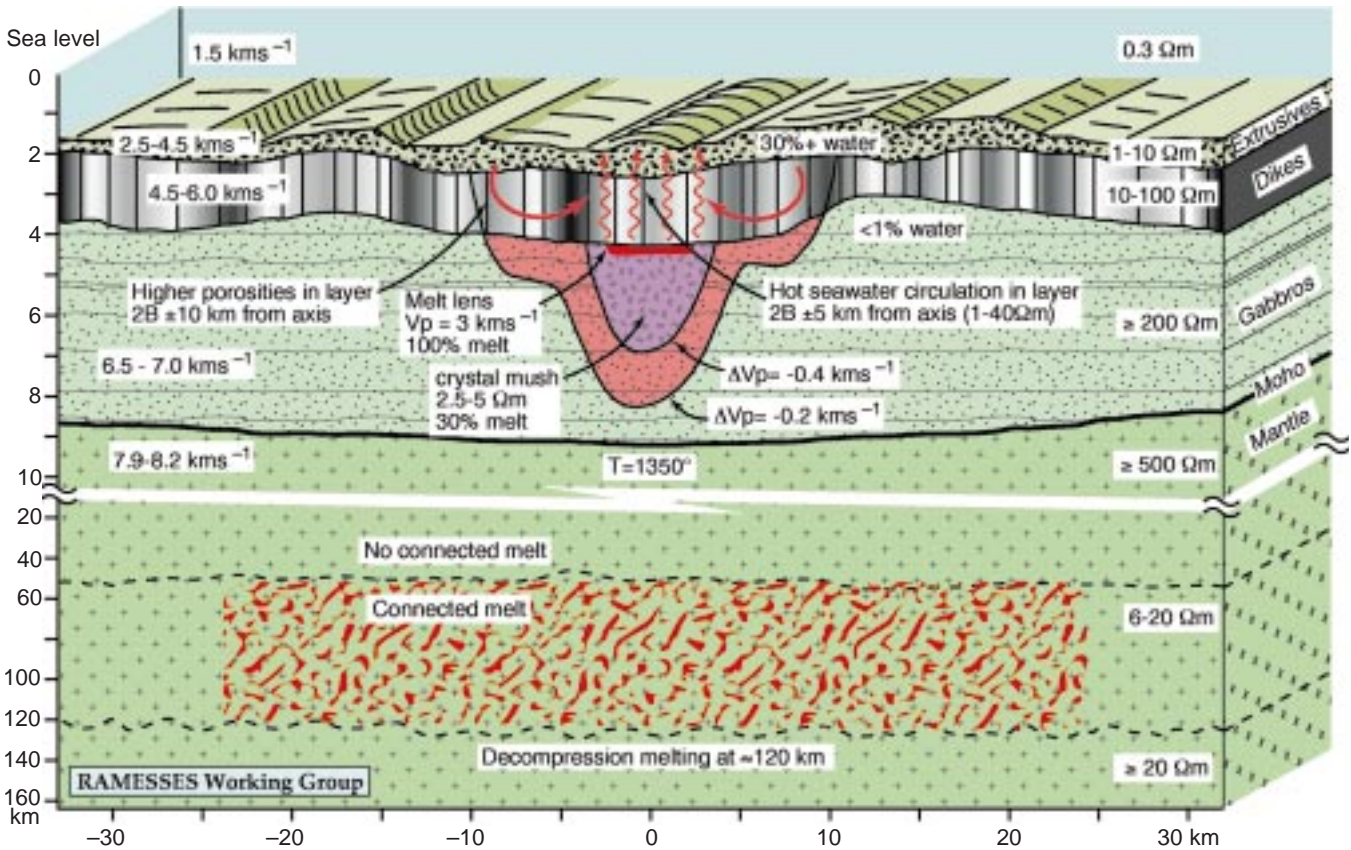


Figure 5. Inferred structural cross-section through the 57°45'N AVR, based on a synthesis of the results from the wide-angle and reflection seismic, controlled-source electromagnetic, and magnetotelluric components of the RAMESSES experiment. The section is drawn along the line of the across-axis wide-angle seismic profile. The seafloor bathymetry and the positions of seismic layer boundaries are quantitatively accurate and are based on swath bathymetry data and seismic modelling. Similarly, estimates of seismic velocities, electrical resistivity, porosity, melt content and temperature are quantitative estimates based on observational data and modelling. Note that a 10:1 break in scale occurs at a depth of 10 km below sea level.

5.1 Porosity structure and aqueous fluids in layer 2

The RAMESSES experiment provides tight constraints on the variation with depth of both P-wave velocity and resistivity in the axial upper crust, allowing us to estimate the extent to which the crust is penetrated by an interconnected aqueous fluid phase. Besides the volume fraction of pore space, the velocity and resistivity are also dependent on pore geometry (for example isolated pore spaces or a connected network of fractures), and on the resistivity of the fluid itself, which depends on its temperature. In the upper few tens of metres of the seafloor at the AVR (layer 2A), both seismic velocity and resistivity are consistent with an interconnected network of void spaces amounting to a total porosity of around 40 per cent, although the very low resistivities are best explained at this value of porosity by a small increase in the temperature of the pore fluid above the ambient sea-water temperature, to perhaps 10°C to 20°C. At such high porosities, a highly connected fluid phase is inevitable. Towards the base of layer 2 beneath the AVR, both velocity and resistivity are still significantly lower than at equivalent depths off-axis. The seismic data are consistent with a 1 to 2 per cent porosity here, at a depth of between 1 and 2 km beneath the seafloor. In order to achieve the observed resistivity with a connected aqueous phase of ambient sea-water temperature and composi-

tion, a higher porosity of at least 4 per cent would be required. This suggests that, at this depth, the temperature of the fluid has been raised considerably above ambient. A well-connected aqueous phase, occupying a total porosity of between 1 and 2 per cent, and at a temperature of between 100 and 200°C (intermediate between ambient and the 360°C typical temperature of black-smoker-type hydrothermal venting) would be consistent with both the seismic and CSEM data for the lower regions of layer 2 at the AVR axis.

At distances of more than 10 to 15 km from the axis, both seismic and CSEM data indicate lower porosities and/or temperatures throughout much of layer 2. Porosity is still high at the seafloor, as evidenced by the 2.5 to 3 km s⁻¹ P-wave velocities typically observed. By the base of layer 2, however, the data are consistent with a decrease to 0.5 per cent porosity or less, and there is no conclusive evidence for significantly raised fluid temperatures.

An unusual feature of the seismic data from this experiment is the sharp step in S-wave velocity between layer 2 and layer 3. This step is required to explain the converted S-wave arrivals seen to occur at consistent time offsets behind the P-wave first arrivals in the across-axis wide-angle data. There is no evidence for a sharp change in P-wave velocity, which instead is modelled as having a change in vertical gradient at this point. Although unusual in oceanic crust, evidence for a similar jump

in S-wave velocity has recently been reported from further north on the Reykjanes Ridge (Smallwood et al. 1995). A possible explanation for this is the vesicular nature of layer 2 basalts observed during drilling into 2.4 Ma old crust at the Reykjanes Ridge at DSDP site 409 (Duffield 1979). The vesicularity is believed to be due to the unusually shallow depth of the Reykjanes Ridge, which allows outgassing of volatiles from the magma as it emerges from the top of the crustal melt body to form dykes or to be erupted. The average vesicularity observed in the DSDP cores—27 per cent—is much higher than the inferred porosity from the geophysical data. It may, however, be the case that most, if not all, of the vesicle spaces are rapidly infilled by secondary mineral growth as the crust ages, and as aqueous fluids circulate through it. Isolated vesicles would have a limited effect on resistivity. They should, however, affect seismic velocity. It is possible that secondary mineral growth results in a composite structure in which the shear modulus remains significantly lower than for the deeper, non-vesicular parts of the crust, while density and bulk modulus approach those of non-vesicular basalts. This could explain the observed shear-wave velocity structure at the layer 2/layer 3 boundary.

5.2 Existence and structure of crustal magma body

The seismic reflection, seismic wide-angle and CSEM data together present overwhelming evidence for a significant crustal melt body beneath the 57°45'N AVR on the Reykjanes Ridge. Seismic constraints show that the body is divided into two distinct regions. The upper part is a ribbon-like lens of very low P-wave velocity, likely to be entirely or very largely filled with basaltic melt, and continuous along-axis for much of the length of the AVR. At the experiment centre, the melt lens is probably 100 m thick, and 4 km wide across-axis.

The lower part of the melt body contains a partially molten, partially crystallized mush, which extends downwards and outwards from the melt lens to within 1 km of the Moho and to a distance of at least 5 km to either side of the axis. The region is broadly wedge shaped, becoming narrower towards its base. The CSEM data put an upper limit on the resistivity over most of this region of 2.5 V m. This would indicate a melt fraction in this zone of at least 20 per cent, and possibly as much as 45 per cent, based on laboratory and modelling constraints (Shankland & Waff 1977; Waff & Weill 1975; Tyburczy & Waff 1983). This is an unexpectedly high melt fraction for a mush zone, which—based on seismic data from Pacific ridges—would be expected to have a melt fraction of only a few per cent. The transformation between P-wave velocity and melt fraction may, however, be unreliable, since the most widely quoted laboratory results by Murase & McBirney (1973) were made at surface pressure, and at least some of the reported drop in P-wave velocities at sub-liquidus temperatures may be due to increased fracturing of the sample as temperature increased. We therefore consider the electrical data to provide more reliable constraints on melt fraction in the mush zone than the seismic data.

The top of the melt body lies exactly at the layer 2/layer 3 seismic boundary, as would be expected if that boundary represented a transition from dominantly dykes and extrusives above to dominantly plutonic rocks below. The observed depth of the melt lens, 2.5 km below the seafloor, is within the range of depths observed for melt lenses beneath the fast spreading

(100 to 140 mm a⁻¹) East Pacific Rise, and is shallower than that observed beneath the intermediate spreading (60 mm a⁻¹) Valu Fa Ridge in the southern Lau Basin. Our results do not, therefore, support the suggestion (Purdy et al. 1992; Phipps Morgan & Chen 1993) that spreading rate is the major determinant of magma chamber depth.

Although the melt body that we have discovered is large, both in terms of its across-axis width and its apparent melt fraction, compared to those found in the Pacific, it is within the range of variation found at faster spreading axes. Above all, the overall geometry—thin, ribbon-like melt lens overlying a larger region of partially crystallized mush—is strikingly similar to the northern and southern East Pacific Rise and the Valu Fa Ridge. The shape of the mush zone, narrowing towards its base, is significantly different from the shape of the seismic low-velocity zones reported beneath the East Pacific Rise near 9°N and 13°N, which are both wedge shaped but with the widest part at the bottom (Harding et al. 1989; Vera et al. 1990). This may reflect real differences in structure, or it may be simply the result of different seismic techniques: an across-axis OBS profile in the RAMESSES experiment, and a set of axis-parallel expanding spread profiles at the East Pacific Rise. Across-axis seismic data from the East Pacific Rise at 9°30'N do not appear to indicate a low-velocity zone that widens downwards (Toomey et al. 1990, 1994).

Our major conclusion, based on the presence of the mid-crustal seismic and resistivity anomaly, is that the process of crustal accretion at this segment of the Mid-Atlantic Ridge does indeed involve the presence of a major, crustal magma body which has much in common in terms of its overall structure, depth and geometry with those previously detected at the East Pacific Rise and the Valu Fa Ridge.

5.3 Volume of melt, residence time and implications for tectono-magmatic cycles

We can use the seismic and electromagnetic constraints on the geometry and properties of the melt body to estimate the total amount of melt present within the crust. The minimum melt fraction of 20 per cent within the mush zone that is compatible with the CSEM data results in an estimate of 3 km³ of melt per along-axis kilometre within the crustal melt body. With knowledge of the crustal thickness and full spreading rate, we can also estimate the mean flux of melt required to generate the crust, which is 1.5×10^{-4} km³ a⁻¹ per along-axis kilometre. The melt currently residing within the crustal magma body therefore represents at least 20 000 years worth of crustal growth. RAMESSES III presents some simple thermal arguments which suggest that the likely cooling time of this melt body to sub-solidus temperatures is only of the order of 1500 years, unless it continues to be supplied from the mantle with fresh magma at a rate that greatly exceeds the steady-state or time-averaged rate needed.

The existence of the melt body beneath a slow spreading ridge, the volume of melt contained within it, the thermal argument that it must represent a non-steady-state feature, and the evidence against magma bodies beneath many other parts of the ridge system together constitute overwhelming evidence that accretion beneath this spreading segment occurs through a cyclic process, involving periodic influxes of melt from the mantle to a crustal magma body. Thus we conclude that crustal accretion here has a similar overall geometry, at

least in some respects, to that at faster spreading rates, but that the melt flux from the mantle is much more strongly modulated through time than at faster spreading rates. The observations are entirely consistent with the model of tectono-magmatic cycles affecting individual AVR segments proposed by Parson et al. (1993). The discovery of the first axial magma body beneath the Mid-Atlantic Ridge at a segment characterized by a volcanically active, but topographically poorly developed, AVR suggests that the tectono-magmatic cycle here follows a pattern similar to that inferred from seismic and bathymetric data at the Valu Fa Ridge by Collier & Sinha (1992a,b). There are, though, some major differences compared to the Valu Fa Ridge. First, the nature of along-axis segmentation is likely to be different. The existing evidence suggests that, at the Reykjanes Ridge, the tectono-magmatic cycle affects the entire AVR, whereas at the Valu Fa Ridge each cycle affects only a 10 to 15 km sub-segment of the ridge. Second, at the VFR it appears that the magma body is rarely, if ever, completely exhausted between melt influxes, whereas at slower spreading rates it appears that the magma body is absent for the majority of the time.

The volume of melt currently present beneath the RAMESSES AVR puts a lower limit of 20 000 years on the period of the tectono-magmatic cycle. If the melt body has already existed for some considerable time, or if the volume of melt exceeds our minimum estimate, or if the melt body is replenished by any further input of melt from the mantle during the course of the current cycle, then the period will increase to greater than 20 000 years. If, as our estimates indicate, the current magma body becomes entirely crystallized in less than 2000 years, then this suggests that within each cycle the crustal magma body is present for less than 10 per cent of the time, and that amagmatic, tectonically dominated extension accounts for spreading for more than 90 per cent of the time. This would readily explain the numerous geophysical observations of amagmatic spreading axes at the Mid-Atlantic Ridge.

Over the course of a 20 000 year cycle, seafloor spreading would result in a total of 400 m of extension. Assuming that this is taken up over a zone 10 km wide (approximately the maximum width of the region currently invaded by crustal magma), then, during the amagmatic phase of extension, we would expect to see crustal thinning of the order of 300 m. Although at the limit of seismic resolution, the suggestion in the best-fitting across-axis wide-angle seismic model that the crust is a few hundred metres thicker at the axis than it is off-axis is again entirely consistent with a model in which the crust has recently grown magmatically, and where the next 20 000+ years will see a period of amagmatic crustal stretching that will reduce axial crustal thickness to the off-axis average.

All of our observations are consistent with the view that crustal accretion at mid-ocean ridges involves the presence of a crustal magma body of broadly similar geometry and properties at all spreading rates, with the major differences associated with spreading rate being confined to the temporal variability of the process, that is, short-lived, transient melt bodies and tectono-magmatic cycles of period 104 to 105 years at slow spreading rates, compared with long-lived or steady-state bodies at faster spreading rates.

Is this conclusion incompatible with inferences from further south on the Mid-Atlantic Ridge (Smith & Cann 1992) that many very small, isolated bodies of magma underlie individual

seamounts? This question is important, because Magde & Smith (1995) report a similar distribution of small seamounts along the southern section of the Reykjanes Ridge to neovolcanic zones on the Mid-Atlantic Ridge at 24° to 30°N. It may be that these observations are not in fact difficult to reconcile. The large crustal magma body is unlikely either to form, or to crystallize, instantly or at a uniform rate beneath the AVR during any tectono-magmatic cycle. Thus during both the early and late stages of the existence of an ephemeral but large crustal magma body, the small fraction of melt present in the crust may be concentrated in small and isolated pockets. Thus the distribution, height and texture of seamounts within the neovolcanic zone would reflect the presence of a crustal melt phase with a time-varying distribution, including both a large and laterally continuous magma body at the peak of the magmatic phase, and possibly much smaller, isolated blobs of melt in the crust during the onset or decay of the magmatic peak.

5.4 Melt production and flow in the mantle

The MT data (Sinha et al. 1997; Heinson et al., in preparation) show at least two distinct regions in the upper mantle. Between the Moho and a depth of about 40 km below sea level, resistivities are relatively high, indicative of a region in which no significant, interconnected melt fraction is present. Beneath this, to a depth of around 120 km, resistivities are depressed below those that would be expected for dry olivine at similar mantle potential temperatures. Resistivities in the deeper region are consistent with the presence of a region of adiabatic, decompression partial melting forming a volumetrically small but interconnected basalt melt phase, with the melt distributed along grain boundaries (e.g. Cheadle 1993).

The MT data, the normal P-wave velocity observed directly beneath the Moho, and the observation of P_P reflections from directly beneath the AVR axis are all consistent with a structural model in which the uppermost few tens of kilometres of the mantle do not contain a partial melt phase. This model is also consistent with the presence of a distinct (even if subdued, compared to further south on the Mid-Atlantic Ridge) median valley at this point on the Reykjanes Ridge. Current geodynamic models (e.g. Chen & Morgan 1990) for the origin of median valleys at slow spreading ridges relate this phenomenon to lithospheric strength and thickness beneath the axis, and in particular to the viscosity of the uppermost mantle. The existence of the median valley here indicates a finite thickness of sub-Moho lithosphere forming an unbroken plate beneath the Reykjanes Ridge axis. Pervasive grain-boundary partial melting would greatly reduce the viscosity, as well as the resistivity and possibly the P-wave velocity, of the uppermost mantle. It appears that the seismic, MT and rheological constraints are all telling a consistent story—that the uppermost few tens of kilometres of the mantle beneath this slow spreading ridge are essentially dry, and that the zone of pervasive, adiabatic, decompression partial melting forming the basaltic magmas that will generate new crust lies at a deeper level.

Two distinct possibilities emerge for the relationship between this currently dry, lithospheric uppermost mantle and the production of basaltic melts. One is that, at certain stages of the tectono-magmatic cycle, this region does act as the source of significant volumes of basaltic magma, by itself undergoing

partial melting. If this is the case, then the current situation beneath the RAMESSES experiment must be explained in terms of the relatively rapid, and recent, draining of at least 20 000 years' worth of magma production from this region. This event has left the uppermost mantle essentially devoid of melt, and instead concentrated the melt into the crustal magma body. If we follow this argument, then we would expect that this part of the mantle would then undergo a steady build-up of a new melt phase, that at some time in the future will again be extracted into the crust to form a new magma body, driving the next tectono-magmatic cycle, in something over 20 000 years time into the future.

An alternative possibility is that the upper few tens of kilometres of the mantle form a permanent lithospheric region, cool enough that no partial melting takes place in this region at any time. All of the melting is confined to the lower region, below 50 km. In this case, the uppermost mantle must provide a conduit through which melt migrates from below to form the crust. Pursuing this model, melt migration in the uppermost mantle must occur through some mechanism other than percolation through a pervasive, grain-boundary network. A system of largely vertical conduits, perhaps a branching system of pipes, fractures, or high-permeability channels (e.g. Richardson, Lister & McKenzie 1996; Kelemen et al. 1997), with little mutual connectivity in a horizontal plane, would be invisible to the MT data, allowing melt to migrate through the uppermost mantle without altering its apparent resistivity. In this case, melt generation may be close to a steady-state process below 50 km depth, but temporal variations in the availability of high-permeability channels through the lithospheric uppermost mantle would drive tectono-magmatic cycles by switching on and off the delivery of melt from below.

The existing geophysical data cannot resolve between these models. Objections based on geochemical or geodynamic modelling can no doubt be raised for either of them. On the other hand, most existing geodynamic and geochemical models for mantle flow and melt production, composition and migration are based on assumptions of quasi-steady-state processes in the mantle, and have difficulty in adequately explaining either the high degree of spatial focusing, or the episodicity, of delivery of basaltic melt into the crustal magma body (e.g. Scott & Stevenson 1989; Parmentier & Phipps Morgan 1990; Forsyth 1992; Spiegelman 1993, 1996). We hope that the RAMESSES results will provide an incentive for re-examining geochemical and geodynamic models, particularly in the context of strongly time-varying distributions of melt within the upper mantle.

Within the 50 to 120 km deep zone of low resistivity in the mantle, the MT data are consistent with a distributed and highly connected basaltic melt phase constituting between 3 and 10 per cent of the total volume. Given the uncertainties in resistivities of the solid and melt phases at the appropriate temperatures and pressures, and on the efficiency of connection of the melt phase, this is not inconsistent with the 1 to 3 per cent partial melt fractions that have been suggested by modelling studies.

5.5 Relation to the Iceland hot spot

The site of our experiment is over 1100 km from the centre of the Iceland plume. At this latitude, a clear median valley extends for more than 100 km northwards towards Iceland

before an axial topographic high appears. The crustal thickness determined seismically is between 7 and 7.5 km—typical of normal oceanic crust. We can infer from this observation that although, at the site of our experiment, the Iceland plume is close enough to cause anomalously shallow water depths and a ridge topography that is atypical of other parts of the Mid-Atlantic Ridge, it is sufficiently distant that it causes no increase in the overall rate of melt production. Other seismic experiments further north on the Reykjanes Ridge (Bunch & Kennett 1980; Smallwood et al. 1995) have failed to find any strong evidence for a crustal melt body, even though they are located closer to the Iceland hot spot, and correspond to locations where abnormally high mantle temperatures cause an increase in overall melt production rates (McKenzie & Bickle 1988; Bown & White 1994), leading to thicker than normal crust. We would therefore argue, based on the normal melt production rate, that what distinguishes the RAMESSES locality from other segments of slow spreading ridges is not its position relative to the Iceland hot spot, but the fact that it is in the most magmatically active stage of its life cycle. Following this argument, we would expect that most AVRs on the Reykjanes Ridge—even those very close to Iceland—would not be underlain by an axial melt body, since such features are short-lived and hence rare. Conversely, we would expect that other slow spreading ridge segments that, like our AVR, are at the most magmatically active stage of their life cycle, might well be underlain by comparable melt bodies, irrespective of their proximity to, or distance from, a hot spot. Hence we believe the results of this study to be representative of the generality of slow spreading ridge segments, but only at a particular, magmatically robust stage in their tectono-magmatic cycle.

6 CONCLUSIONS

In combination, the geophysical results from the RAMESSES experiment provide convincing evidence for a significant volume of magmatic fluid beneath the 57°45'N AVR segment of the Reykjanes Ridge, both within the crust and at depths greater than 50 km in the mantle. The discussion in Sections

4 and 5 is summarized below.

(1) The AVR is underlain by a significant crustal melt body. This appears to have many broad similarities (depth below the sea surface, vertical and across-axis dimensions, and internal structure consisting of a thin, ribbon-like melt lens flanked and underlain by a larger, axial low-velocity region) to those seen beneath faster spreading ridges in the Pacific.

(2) Although the basic geometry of melt accumulation and emplacement here appears similar to that at higher spreading rates, the patterns of along-axis and temporal variations differ.

(3) Crustal accretion is controlled by tectono-magmatic cycles affecting individual AVR segments. The period of this cycle is at least 20 000 years, and a crustal magma body is present for only a small (probably 10 per cent or less) proportion of each cycle. For the remainder of each cycle, seafloor spreading is accommodated by amagmatic crustal extension, during which the volcanically constructed AVRs are destroyed by the growth of spreading-orthogonal normal faults.

(4) The seismic evidence for normal (7 to 7.5 km) thickness crust shows that the rate of melt production here is typical of that found elsewhere on the mid-ocean ridge system. The

magmatic flux here is no greater than it is further south on the Mid-Atlantic Ridge, where crust of similar thickness is produced at the same or higher spreading rates. So, what distinguishes this locality from other segments of slow spreading ridges is not its position relative to the Iceland hot spot, but the fact that it is in the most magmatically active stage of its life cycle.

(5) The low seismic velocities and extremely low resistivities observed in the upper part of the crust beneath the AVR indicate the presence of a high porosity and a highly connected aqueous fluid phase. At the axis, this fluid is at temperatures significantly above that of ambient sea water. It seems probable that the 57°45'N AVR should be the site of vigorous hydrothermal venting.

(6) The upper 40 km of the mantle contains no detectable interconnected melt phase, and must therefore be experiencing sub-solidus conditions. It is possible that this region has recently been drained of melt, which has then accumulated in the crustal magma body. Alternatively, this part of the mantle does not experience melting, and hence upward-migrating magma must pass through it on the way to the crust by means of some non-porous flow.

(7) The mantle at depths of between 50 and 120 km below the sea surface is characterized by low resistivities of less than 50 V m, indicative of the presence of a small volumetric fraction

of interconnected partial melt.

Finally, the RAMESSES experiment has provided a demonstration of the power of an integrated, geophysical approach combining a range of techniques. Wide-angle and normal-incidence seismic, CSEM and MT results have all provided essential constraints without which we would have been unable to produce the composite structural model shown in Fig. 5. RAMESSES is the first such integrated experiment to have been carried out anywhere in the oceans, and its success relied on close collaboration between four research groups in three continents, beginning considerably before the experimental work at sea, and continuing for at least four years thereafter. The other key factor in this study was its careful targeting on a selected spreading segment, made possible by the existence of high-resolution, regional-scale sonar mapping data. Diversity of approaches and techniques is clearly essential to progress in this area of research, but concentration of the efforts of several groups in a coherent and integrated study can, in the correct circumstances, provide the best opportunities

for new understanding of ridge processes.

ACKNOWLEDGMENTS

We would like to thank the officers and crew of RRS Charles Darwin, the sea-going technical staff of NERC Research Vessel Services, and other members of the scientific party of Cruise CD81 for their assistance and support during a complex, demanding and crowded experimental programme. We also thank Roger Searle for extremely useful discussions and access to TOBI side-scan data during the selection of our target AVR. Many other people contributed directly or indirectly to the conception and execution of the RAMESSES experiment, and we wish to thank them all for their efforts. This work was supported by the UK's Natural Environment Research Council in the form of research grant GR3/8032, ship time (CD81/93) and two PhD studentships (DAN & LMM), by the US

National Science Foundation (OCE 91-02551) and by the Australian Research Council. Maps were plotted using the

GMT programs of Wessel & Smith (1995).

REFERENCES

- Bown, J.W. & White, R.S., 1994. Variation with spreading rate of oceanic crustal thickness and geochemistry, *Earth Planet. Sci. Lett.*, **121**, 435–449.
- Bunch, A.W.H. & Kennett, B.L.N., 1980. The crustal structure of the Reykjanes Ridge at 59°30'N, *Geophys. J. R. astr. Soc.*, **61**, 141–146.
- Calvert, A.J., 1995. Seismic evidence for a magma chamber beneath the slow-spreading Mid-Atlantic Ridge, *Nature*, **377**, 410–414.
- Calvert, A.J., 1997. Backscattered coherent noise and seismic reflection imaging of the oceanic crust: An example from the rift valley of the Mid-Atlantic Ridge at 23°N, *J. geophys. Res.*, **102**, 5119–5133.
- Cann, J.R., 1974. A model for oceanic coastal structure developed, *Geophys. J. R. astr. Soc.*, **39**, 169–187.
- Cheadle, M.J., 1993. The physical properties of texturally equilibrated partially molten rocks, *EOS, Trans. Am. geophys. Un.*, **74**, 283.
- Chen, Y. & Morgan, W.J., 1990. Rift valley/no rift valley transition at mid-ocean ridges, *J. geophys. Res.*, **95**, 17 571–17 581.
- Collier, J.S. & Sinha, M.C., 1992a. Seismic mapping of a magma chamber beneath the Valu Fa Ridge, Lau Basin, *J. geophys. Res.*, **97**, 14 031–14 053.
- Collier, J.S. & Sinha, M.C., 1992b. The Valu Fa Ridge: the pattern of volcanic activity at a back-arc spreading centre, *Mar. Geol.*, **104**, 243–263.
- Constable, S.C. & Cox, C.S., 1996. Marine controlled-source electromagnetic sounding II: The PEGASUS experiment, *J. geophys. Res.*, **101**, 5519–5530.
- Constable, S.C., Shankland, T.J. & Duba, A., 1992. The electrical conductivity of an isotropic olivine mantle, *J. geophys. Res.*, **97**, 3397–3404.
- DeMets, C., Gordon, R.G., Argus, D.F. & Stein, S., 1990. Current plate motions, *Geophys. J. Int.*, **101**, 425–478.
- Detrick, R.S., Buhl, P., Vera, E., Mutter, J., Orcutt, J., Madsen, J. & Brocher, T., 1987. Multi-channel seismic imaging of a crustal magma chamber along the East Pacific Rise, *Nature*, **326**, 35–42.
- Detrick, R.S., Mutter, J.C., Buhl, P. & Kim, I., 1990. No evidence from multichannel reflection data for a crustal magma chamber in the MARK area on the Mid-Atlantic Ridge, *Nature*, **347**, 61–64.
- Detrick, R.S., Harding, A.J., Kent, G.M., Orcutt, J.A., Mutter, J.C. & Buhl, P., 1993. Seismic structure of the southern East Pacific Rise, *Science*, **259**, 499–503.
- Duffield, W.A., 1979. Significance of contrasting vesicularity in basalt from DSDP holes 407, 408 and 409 on the west flanks of the Reykjanes Ridge, *Init. Rep. Deep Sea Drill. Proj.*, **49**, 715–719.
- Forsyth, D.W., 1992. Geophysical constraints on mantle flow and melt generation beneath mid-ocean ridges, in *Mantle Flow and Melt Generation at Mid-Ocean Ridges*, pp. 103–122, *Geophysical Monograph 71*, AGU, Washington, DC.
- Fowler, C.M.R., 1976. Crustal structure of the Mid-Atlantic Ridge crest at 37°N, *Geophys. J. R. astr. Soc.*, **47**, 459–491.
- Fowler, C.M.R. & Keen, C.E., 1979. Oceanic crustal structure—Mid-Atlantic Ridge crest at 45°N, *Geophys. J. R. astr. Soc.*, **56**, 219–226.
- Harding, A.J., Orcutt, J.A., Kappus, M.E., Vera, E.E., Mutter, J.C., Buhl, P., Detrick, R.S. & Brocher, T.M., 1989. The structure of young oceanic crust at 13°N on the East Pacific Rise from expanding spread profiles, *J. geophys. Res.*, **94**, 12 163–12 196.
- Henstock, T.J., Woods, A.W. & White, R.S., 1993. The accretion of oceanic crust by episodic sill intrusion, *J. geophys. Res.*, **98**, 4143–4161.
- Keeton, J.A., Searle, R.C., Parsons, B., White, R.S., Murton, B.J., Parson, L.M., Peirce, C. & Sinha, M., 1997. Bathymetry of the Reykjanes Ridge, *Mar. Geophys. Res.*, **19**, 55–64 (plus set of 4 maps).
- Kelemen, P.B., Hirth, G., Shimizu, N., Spiegelman, M. & Dick, H.J.B.,

1997. A review of melt migration processes in the adiabatically upwelling mantle beneath oceanic spreading ridges, *Phil. Trans. R. Soc. Lond., A*, **355**, 283–318.
- Kuszniir, N.J. & Bott, M.H.P., 1976. A thermal study of the formation of oceanic crust, *Geophys. J. R. astr. Soc.*, **47**, 83–95.
- MacGregor, L.M., Constable, S. & Sinha, M.C., 1998. The RAMESSES experiment—III. Controlled-source electromagnetic sounding of the Reykjanes Ridge at 57°45'N, *Geophys. J. Int.*, **135**, 773–789 (this issue).
- McKenzie, D.P. & Bickle, M.J., 1988. The volume and composition of melt generated by extension of the lithosphere, *J. Petrol.*, **29**, 625–675.
- Magde, L.S. & Smith, D.K., 1995. Seamount-volcanism at the Reykjanes Ridge: Relationship to the Iceland hot spot, *J. geophys. Res.*, **100**, 8449–8468.
- Murase, T. & McBirney, A.R., 1973. Properties of some common igneous rocks and their melts at high temperatures, *Geol. Soc. Am. Bull.*, **84**, 3563–3592.
- Murton, B.J. & Parson, L.M., 1993. Segmentation, volcanism and deformation of oblique spreading centres: a quantitative study of the Reykjanes Ridge, *Tectonophysics*, **222**, 237–257.
- Navin, D.A., Peirce, C. & Sinha, M.C., 1998. The RAMESSES experiment—II. Evidence for accumulated melt beneath a slow spreading ridge from wide-angle refraction and multichannel reflection seismic profiles, *Geophys. J. Int.*, **135**, 746–772 (this issue).
- Parmentier, E.M. & Phipps Morgan, J., 1990. The spreading-rate dependence of three-dimensional spreading centre structure, *Nature*, **348**, 325–328.
- Parson, L.M. et al. 1993. En echelon axial volcanic ridges at the Reykjanes Ridge: a life cycle of volcanism and tectonics, *Earth planet. Sci. Lett.*, **117**, 73–87.
- Phipps Morgan, J. & Chen, Y.J., 1993. The genesis of oceanic crust: magma injection, hydrothermal circulation, and crustal flow, *J. geophys. Res.*, **98**, 6283–6297.
- Purdy, G.M. & Detrick, R.S., 1986. Crustal structure of the Mid-Atlantic Ridge at 23°N from seismic refraction studies, *J. geophys. Res.*, **91**, 3739–3762.
- Purdy, G.M., Kong, L.S.L., Christeson, G.L. & Solomon, S.C., 1992. Relationship between spreading rate and the seismic structure of mid-ocean ridges, *Nature*, **355**, 815–817.
- Richardson, C.N., Lister, J.R. & McKenzie, D., 1996. Melt conduits in a viscous, porous matrix, *J. geophys. Res.*, **101**, 20 423–20 432.
- Schilling, J.G., Zajac, M., Evans, R., Johnston, T., White, W., Devine, J.D. & Kingsley, R., 1983. Petrologic and geochemical variations along the Mid-Atlantic Ridge from 29°N to 73°N, *Am. J. Sci.*, **283**, 510–586.
- Scott, D. & Stevenson, D., 1989. A self-consistent model of melting, melt migration and buoyancy-driven circulation beneath mid-ocean ridges, *J. geophys. Res.*, **94**, 2973–2988.
- Searle, R.C. & Laughton, A.S., 1981. Fine scale sonar study of tectonics and volcanism on the Reykjanes Ridge, *Oceanologica Acta*, **4**, 5–13.
- Searle, R.C., Field, P.R. & Owens, R.B., 1994. Segmentation and a non-transform ridge offset on the Reykjanes Ridge near 58°N, *J. geophys. Res.*, **99**, 24 159–24 172.
- Shankland, T.J. & Waff, H.S., 1977. Partial melting and electrical conductivity anomalies in the upper mantle, *J. geophys. Res.*, **82**, 5409–5417.
- Sinha, M.C., Patel, P.D., Unsworth, M.J., Owen, T.R.E. & MacCormack, M.R.G., 1990. An active source electromagnetic sounding system for marine use, *Mar. geophys. Res.*, **12**, 59–68.
- Sinha, M., Peirce, C., Constable, S. & White, A., 1994. An integrated geophysical investigation of the axial volcanic region of the Reykjanes Ridge at 57°45'N—RRS Charles Darwin 81 Cruise Report, University of Cambridge.
- Sinha, M.C., Navin, D.A., MacGregor, L.M., Constable, S., Peirce, C., White, A., Heinson, G. & Inglis, M.A., 1997. Evidence for accumulated melt beneath the slow-spreading Mid-Atlantic Ridge, *Phil. Trans. R. Soc. Lond., A*, **355**, 233–253.
- Sinton, J.M. & Detrick, R.S., 1992. Mid-ocean ridge magma chambers, *J. geophys. Res.*, **97**, 197–216.
- Sleep, N.H., 1975. Formation of oceanic crust: some thermal constraints, *J. geophys. Res.*, **80**, 4037–4042.
- Smallwood, J.R., White, R.S. & Minshull, T.A., 1995. Sea-floor spreading in the presence of the Iceland plume: the structure of the Reykjanes Ridge at 61°40'N, *J. geol. Soc.*, **152**, 1023–1029.
- Smith, D.K. & Cann, J.R., 1992. The role of volcanism in crustal construction at the Mid-Atlantic Ridge (24°–30°N), *J. geophys. Res.*, **97**, 1645–1658.
- Spiegelman, M., 1993. Physics of melt extraction: theory, implications and applications, *Phil. Trans. R. Soc. Lond., A*, **342**, 23–41.
- Spiegelman, M., 1996. Geochemical consequences of melt transport in 2-D: the sensitivity of trace elements to mantle dynamics, *Earth planet. Sci. Lett.*, **139**, 115–132.
- Taylor, R.N., Murton, B.J. & Thirlwall, M.F., 1995. Petrographic and geochemical variation along the Reykjanes Ridge, 57°–59°N, *J. geol. Soc. Lond.*, **152**, 1031–1037.
- Toomey, D.R., Purdy, G.M., Solomon, S.C. & Wilcock, W.S.D., 1990. The three-dimensional seismic velocity structure of the East Pacific Rise near latitude 9°30'N, *Nature*, **347**, 639–645.
- Toomey, D.R., Solomon, S.C. & Purdy, G.M., 1994. Tomographic imaging of the shallow crustal structure of the East Pacific Rise at 9°30'N, *J. geophys. Res.*, **99**, 24 135–24 157.
- Tyburczy, J.A. & Waff, H.S., 1983. Electrical conductivity of molten basalt and andesite to 25 kilobars pressure: geophysical significance and implications for charge transport and melt structure, *J. geophys. Res.*, **88**, 2413–2430.
- Unsworth, M.J., 1994. Exploration of mid-ocean ridges with a frequency-domain electromagnetic system, *Geophys. J. Int.*, **116**, 447–467.
- Vera, E.E., Mutter, J.C., Buhl, P., Orcutt, J.A., Harding, A.J., Kappus, M.E., Detrick, R.S. & Brocher, T.M., 1990. Structure of 0- to 0.2-m.y. old oceanic crust at 9°N on the East Pacific Rise from expanded spread profiles, *J. geophys. Res.*, **95**, 15 529–15 556.
- Waff, H.S. & Weill, D.F., 1975. Electrical conductivity of magmatic liquids: effects of temperature, oxygen fugacity and composition, *Earth planet. Sci. Lett.*, **28**, 254–260.
- Wessel, P. & Smith, W.H.F., 1995. New version of the Generic Mapping Tools released. EOS, *Trans. Am. geophys. Un.*, **76**, 329.
- White, R.S., McKenzie, D. & O'Nions, R.K., 1992. Oceanic crustal thickness from seismic measurements and rare earth element inversions, *J. geophys. Res.*, **97**, 19 683–19 715.
- Wolfe, C.J., Purdy, G.M., Toomey, D.R. & Solomon, S.C., 1995. Microearthquake characteristics and crustal velocity structure at 29°N on the Mid-Atlantic Ridge: The architecture of a slow-